Design of wide band-pass substrate integrated waveguide (SIW) filters based on stepped impedances

Clara Máximo-Gutiérrez[a], Juan Hinojosa[b] and Alejandro Alvarez-Melcon[a]

Affiliations and email addresses:

[a]MSc. Clara Máximo-Gutiérrez

Universidad Politécnica de Cartagena

Department of Information and Communications Technology

Campus Universitario Muralla del Mar

Plaza del Hospital, 1

30202 Cartagena (Murcia) – Spain.

Email: clara_maximo@hotmail.com

[b]Dr. Juan Hinojosa

Universidad Politécnica de Cartagena

Department of Electronics and Computer Engineering

Campus Universitario Muralla del Mar

Plaza del Hospital, 1

30202 Cartagena (Murcia) – Spain.

Email: juan.hinojosa@upct.es

[a]Dr. Alejandro Alvarez-Melcon

Universidad Politécnica de Cartagena

Department of Information and Communications Technology

Campus Universitario Muralla del Mar

Plaza del Hospital, 1

30202 Cartagena (Murcia) – Spain.

Email: alejandro.alvarez@upct.es

Corresponding author: Dr. Alejandro Alvarez-Melcon

Email: alejandro.alvarez@upct.es

Phone: + 34 968 32 53 15

ABSTRACT:

A full-wave design technique of *n*-order Chebyshev stepped impedance band-pass filters in substrate integrated waveguide (SIW) is presented for the first time. The structure of the filter is based on including elliptic patterns etched on the SIW top surface to synthesize Chebyshev transfer functions. The band-pass response is obtained from the high-pass characteristic of the SIW line together with the behavior of the elliptic patterns, which implement the impedance inverters needed to control an upper cut-off frequency in the response of the filter. The synthesis technique is applied to the design of a sixth-order Chebyshev stepped impedance band-pass SIW filter. It is shown that the use of elliptic patterns instead of circular patterns can increase the spurious free range of the filter. In addition, when exponential microstrip-to-SIW transitions are integrated into the design process, a reduction in size and improvement in return loss are achieved, as compared to a base-line filter (sixth-order Chebyshev stepped impedance band-pass filter) designed with transitions separately. Electromagnetic (EM) simulation and measurements results have shown the effectiveness of the proposed design technique to carry out high-performance band-pass filters in SIW technology.

Keywords: Band-pass filter, Filter synthesis, Substrate integrated waveguide (SIW)

1. Introduction

In modern communication systems for satellite and mobile applications, high-performance RF/microwave filters with stringent requirements in terms of weight, cost, insertion loss, quality factor and power handling capability are required [1]. The substrate integrated waveguide (SIW) is a recent technology that can fulfill these requirements [2-9] and also has a great potential for the development of broadband systems. Its operation principle is similar to a rectangular waveguide loaded with a dielectric material. Hence, the SIW technology allows to implement a wide range of circuits based on classical rectangular waveguide by using inductive discontinuities [10]. In addition, the SIW structure is compatible with planar technology which facilitates the integration of a wide range of passive and active planar devices in the same circuit.

In the last years, there has been a great interest to implement band-pass filters in SIW technology. In addition to conventional inductive discontinuities [10], band-pass SIW filters can be obtained by means of electromagnetic bandgap structures (EBGs) [11-14], defected ground structures (DGSs) [15-17], perforated sections (PSs) [18,19] or different types of resonators [20,21], including split ring resonators (SRRs) [22-26]. Many of these band-pass SIW filters use a similar design method that combines the high-pass characteristic of the SIW line and the stop-band behavior of some discontinuities or resonators in cascade to accomplish a band-pass response [11-14,17], [20-25]. In this way, it is possible to achieve band-pass SIW filters with different bandwidths (small or large). However, this design method does not allow to define with accuracy the bandwidth, and the precise electrical characteristics inside the passband. It requires an optimization of the full filter structure to align its response with the initial design specifications. This design method is not computationally efficient, since the design time increases for three-dimensional (3D) structures and even more when the number of discontinuities or resonators in cascade is incremented. The design methods of band-pass

SIW filters based on *LC* resonators lead to small bandwidths (FBW < 10 %) [15,16,26], since their synthesis use lumped-element equivalent circuits which are valid in a narrow band. Other design methods of band-pass filters model perforated SIW sections as impedance inverters, and the SIW line sections as $\lambda_g/2$ resonators [18,19]. Their synthesis technique uses distributed resonators, and they allow to carry out larger bandwidths (FBW < 21 %) than the methods based on lumped *LC* resonators. However, due to the high quality factor of the resonators, the sensitivity of the structure is usually high, especially for narrowband filters. On the contrary, the design methods of stepped impedance filters are rigorous and simpler. They allow achieving wider bandwidths, since they use transmission line sections and impedance inverters to adjust an upper cut-off in the filter transfer function. Moreover, the stepped impedance structures are less sensitivity to mechanical tolerances than their band-pass counterparts, since they do not require the use of resonators. However, the possibilities of implementing band-pass filters exploiting the high-pass characteristic of the SIW together with the stepped impedance synthesis technique have not yet been explored in detail.

In this paper, this technological gap is filled by designing for the first time a high-performance band-pass filter in SIW technology by means of a full-wave stepped impedance synthesis technique and two strategies. The stepped impedance synthesis technique is applied to the implementation of Chebyshev transfer functions. The different impedance sections are converted to sections of equal impedance by using impedance inverters, as shown in [27]. These impedance inverters are implemented by means of elliptic patterns etched on the top surface of the SIW instead of circular ones, as indicated in the structure presented in Fig. 1. It is shown that this first design strategy has the ability to increase the spurious free range of the filter. Traditionally, SIW filters are first designed using ideal waveguide ports. When the design is completed, tapered microstrip-to-SIW transitions are added for integration with microstrip circuits [28]. These transitions transform the quasi-TEM mode of the microstrip line into the

TE_{10} mode of the SIW line. However, these transitions are long and only have good performance in a limited bandwidth. Consequently, the size and performance of the SIW filter are, respectively, increased and degraded by these transitions. To overcome this problem, in this work we propose to replace the tapered microstrip-to-SIW transition by one more compact, and integrate it into the design process as part of the first and last impedance inverters. Applying this second design strategy to a compact exponential microstrip-to-SIW transition, the return loss of the final structure can be improved, and at the same time the overall size of the filter is reduced.

In this paper, the design approach of band-pass SIW filters is first described. The high-pass characteristic of the SIW line defines the lower cut-off frequency of the band-pass response ($f_{c,L}$), while a full-wave stepped impedance synthesis method including the two previous strategies achieves the higher cut-off frequency ($f_{c,H}$). In order to illustrate the performance of our design method, a sixth-order band-pass filter based on stepped impedances and Chebyshev functions has been fabricated and measured, and carefully compared with respect to a base-line filter. The base-line filter is also a sixth-order Chebyshev stepped impedance band-pass SIW filter, which has been first designed using ideal waveguide ports, and then tapered microstrip-to-SIW transitions have been added [28]. Simulated and measured results have shown a good agreement, and the predicted improvements in terms of performance and reduction in size have been demonstrated. This proposed method can be useful for the effective design of high-performance band-pass filters in SIW technology.

2. Design of band-pass SIW filters based on stepped impedances

The proposed design method of band-pass SIW filters (Fig. 1) combines the high-pass characteristic of the SIW and a stepped impedance synthesis method to obtain, respectively, the desired lower ($f_{c,L}$) and higher ($f_{c,H}$) cut-off frequencies of the pass-band. The lower cut-off frequency of the pass-band SIW response ($f_{c,L}$) is obtained by optimizing the width W_{SIW} of the SIW line through the well-known empirical relationships defined in [4], while the higher cut-off frequency ($f_{c,H}$) is achieved by applying a synthesis method for stepped impedance filters synthesizing a Chebyshev transfer function. The technique follows similar concepts to those used for the stepped impedance low-pass filter prototype in rectangular waveguide discussed in [27]. The sections with different characteristic impedances (Fig. 2(a)) are transformed into sections of equal characteristic impedances by using intermediate impedance inverters (Fig. 2(b)). The proposed synthesis method is applied to the design of a sixth-order Chebyshev stepped impedance band-pass filter. Elliptic patterns (Fig. 1) are etched on the top metallic surface to implement the impedance inverters. A major-minor axis ratio of $3R_i/2$ (i = 1, …, 4) was considered in the design of the ellipse in order to have a compromise between the interactions of the contiguous elliptic patterns and the two lateral metallic cylinder rows of via-holes. For integration with microstrip circuits, a compact exponential microstrip-to-SIW transition (Fig. 1) is added in both ports of the band-pass SIW filter. To improve the overall performance of the band-pass SIW filter we propose to include the effects of the transitions as part of the design process, as it will be described in this paper. The integration of the transition as part of the first/last impedance inverter ensures that the designed band-pass filter performs closely within the initial design specifications. This does not occur if the filter is designed first using ideal waveguide ports, and then the transitions are added afterwards. In this case, we have verified that the interactions of the filter and the transitions can degrade considerably the overall performance of the filter, as it will be shown in the next section.

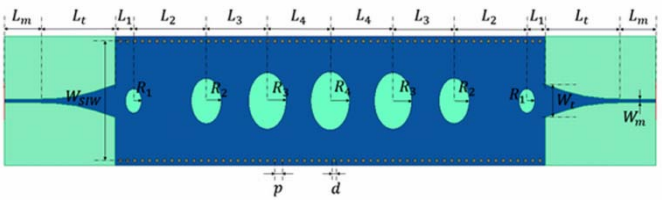

Fig. 1. Structure of the sixth-order Chebyshev stepped impedance band-pass SIW filter with elliptic patterns and exponential microstrip-to-SIW transitions.

The design method of band-pass SIW filters based on stepped impedances and Chebyshev functions is started by computing the width W_{SIW} of the SIW line by means of empirical relationships [4] and the lower cut-off frequency ($f_{c,L}$) of the pass-band, which is given in the initial design specifications (shown in Table 1).

$$W_{SIW} = \frac{c}{2f_{c,L}\sqrt{\varepsilon_r}} + \frac{d^2}{0.95p} \tag{1}$$

where c, ε_r, d and p are, respectively, the speed of light in free space, the relative permittivity of the substrate, the diameter of the metalized via-holes and the pitch length between metalized via-holes (Fig. 1). This approximation is valid for $p < 4\,d$ and $p < \lambda_0\sqrt{\epsilon_r}/2$.

Table 1

Initial design specifications of the Chebyshev stepped impedance SIW filter.

Parameter	Value
Order	6
Return loss, *RL* (dB)	20
Lower cut-off frequency at $\|S_{11}\|$ = - 20 dB, $f_{c,L}$ (GHz)	3
Higher cut-off frequency at $\|S_{11}\|$ = -20 dB, $f_{c,H}$ (GHz)	3.9
Cut-off angle, θ_c (º)	25
Substrate permittivity, ε_r	10.2
Substrate thickness, *h* (mm)	0.635
Diameter of the metalized via-holes, *d* (mm)	0.6
Pitch length between metalized via-holes, *p* (mm)	1.2

Then, the proposed Chebyshev stepped impedance synthesis method [27] is applied to design the target transfer function according to the design specifications given in Table 1. The transfer and reflection functions of the filter, based on sixth-degree Chebyshev polynomials, are first computed. The 6th-order stepped impedance filter (Fig. 2(a)) is first synthesized by cascading six transmission lines of the same length θ_c, but with different characteristic impedances (Z_i). The value of the different characteristic impedances is analytically obtained with an iterative extraction algorithm [27], applied to the [ABCD] matrix of the circuit with the previous transfer and reflection functions. Next, for a practical implementation, the circuit of cascaded transmission lines (Fig. 2(a)) is transformed to another circuit (Fig. 2(b)), defined by six transmission lines with the same characteristic impedance and electrical length θ_c, and different impedance inverters. The impedance inverters are scaled according to their adjacent impedances as:

$$K_{i,i+1} = \frac{1}{\sqrt{Z_i Z_{i+1}}} \quad i = 0, 1, \cdots, N \qquad Z_i = \begin{cases} Z_i & \text{if } i \text{ is odd} \\ 1/Z_i & \text{if } i \text{ is even} \end{cases} \tag{2}$$

where $Z_0 = Z_s = Z_{01} = 1$ and $Z_{N+1} = Z_L = Z_{02} = 1$ (Fig. 2(b)).

The element values of the normalized characteristic impedances and impedance inverters of Fig. 2 are given in Table 2 for the initial design specifications of the sixth-order Chebyshev stepped impedance filter (Table 1) to be implemented.

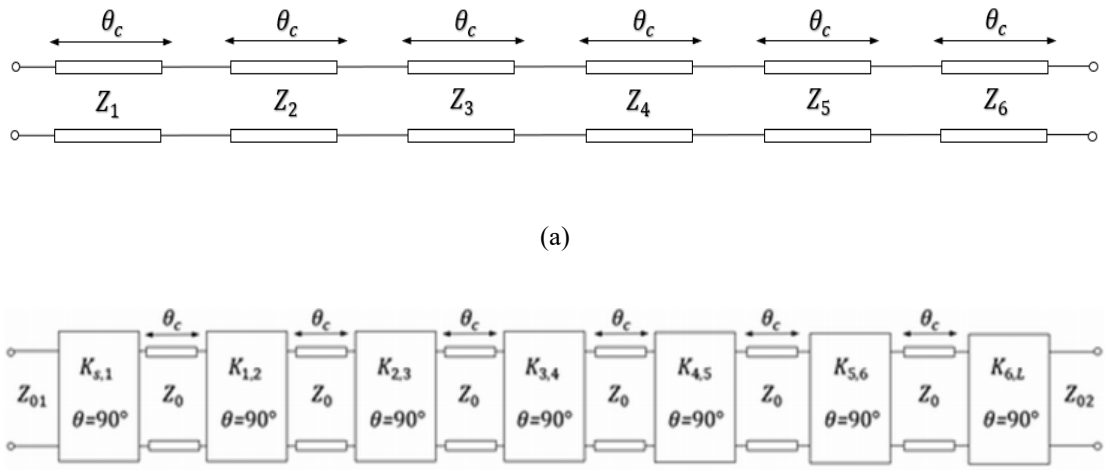

Fig. 2. Synthesis of a sixth-order Chebyshev stepped impedance filter. (a) Filter implemented by means of stepped impedance transmission lines. (b) Filter implemented by means of equal sections of transmission lines and impedance inverters.

Table 2

Normalized element values of the sixth-order Chebyshev stepped impedance SIW filter.

Parameter	Value	Parameter	Value
Z_1	2.4171	$K_{S,1}$	0.6246
Z_2	0.3295	$K_{1,2}$	0.3653
Z_3	4.1708	$K_{2,3}$	0.2748
Z_4	0.2930	$K_{3,4}$	0.2669
Z_5	3.7089	$K_{4,5}$	0.2748
Z_6	0.5057	$K_{5,6}$	0.3653
		$K_{6,L}$	0.6246

The final design of the sixth-order band-pass filter (Fig. 1) was realized by means of a commercial full-wave 3D electromagnetic (EM) simulator (Ansys HFSS). The transmission lines and the impedance inverters (Fig. 2(b)) were implemented by means of the two sections of the filter structure depicted in Fig. 3. The first section depicted in Fig 3(a) has two SIW lines of length *L*/2 (electrical length $\theta_c/2$, in Table 1) and an elliptic pattern (*R*), which implements an impedance inverter. In Fig. 3(b), the second section additionally includes an exponential microstrip-to-SIW transition as part of the first and last impedance inverters. For the design of the sixth-order band-pass filter (Fig. 1), the *S*-parameters obtained from equations (3)-(5) were optimized to match the values obtained in the synthesis method (given in Table 2), adjusting the parameters R_i of the ellipse, the lengths L_i of the two SIW lines and the dimensions of the exponential microstrip-to-SIW transition.

$$S_{22} = \frac{K/\sqrt{Z_{01}Z_{02}} - \sqrt{Z_{01}Z_{02}}/K}{K/\sqrt{Z_{01}Z_{02}} + \sqrt{Z_{01}Z_{02}}/K} \tag{3}$$

$$S_{21} = \frac{2}{j(K/\sqrt{Z_{01}Z_{02}} + \sqrt{Z_{01}Z_{02}}/K)} \tag{4}$$

$$S_T = \begin{bmatrix} e^{-j\theta_c/2} & 0 \\ 0 & e^{-j\theta_c/2} \end{bmatrix} \cdot \begin{bmatrix} S_{11} & S_{12} \\ S_{21} & S_{22} \end{bmatrix} \cdot \begin{bmatrix} e^{-j\theta_c/2} & 0 \\ 0 & e^{-j\theta_c/2} \end{bmatrix} \quad (5)$$

The relationships (3) and (4) correspond to the scattering parameters of an isolated impedance inverter (K) with reference impedances (Z_{01}, Z_{02}), while (5) refers to the scattering parameters once the terminal transmission lines of electrical length $\theta_c/2$ are added on both sides. The design process of the section (impedance inverter without transition) shown in Fig. 3(a) is carried out in two steps:

Step 1) The parameter R_i of the ellipse is varied to produce the value of the magnitude of the S_{21} parameter calculated from equation (4), to synthesize normalized impedance inverters given in Table 2. Fig. 4(a) shows the magnitude of the S_{21} parameter for the section of Fig. 3(a) as a function of the parameter R_i of the ellipse, calculated at the upper cut-off frequency. The parameter R_i of all the impedance inverters of the filter shown in Fig. 3(a) can be easily obtained by means of the graphic depicted in Fig. 4(a).

Step 2) The physical length of the transmission lines ($L_i/2$) corresponding to the electrical length ($\theta_c/2$) of the equivalent network is computed. The phase of the S_{21} parameter for an ideal inverter terminated with two transmission lines of length ($\theta_c/2$) is calculated as: $\varphi(S_{21}) = -90° - \theta_c = -115°$ ($\theta_c = 25°$, Table 1). In Fig. 4(b) we present the phase of the S_{21} parameter computed at the upper cut-off frequency, for the structure shown in Fig. 3(a) as a function of the length (L_i). The length L_i of all transmission line sections of the filter shown in Fig. 3(a) can be easily determined with the information provided by the graphic of Fig. 4(b).

The parameter R_1 and the length L_1 of the first/last section (impedance inverter with transition) of the filter shown in Fig. 3(b) are obtained in a similar way. The design process of the section shown in Fig. 3(b) slightly differs to previous one in the second step, since the impedances Z_{01}

and Z_{02} (Fig. 3(b)) are not equal at both ports. Therefore, the length L_1 of the first/last transmission line section can only be adjusted by using the phase of the S_{22} parameter obtained in the synthesis through equations (3) and (5). The phase of the S_{22} parameter for an ideal impedance inverter terminated with a transmission line of length $(\theta_c/2)$ is $\varphi(S_{22}) = -\theta_c = -25°$ (Table 1).

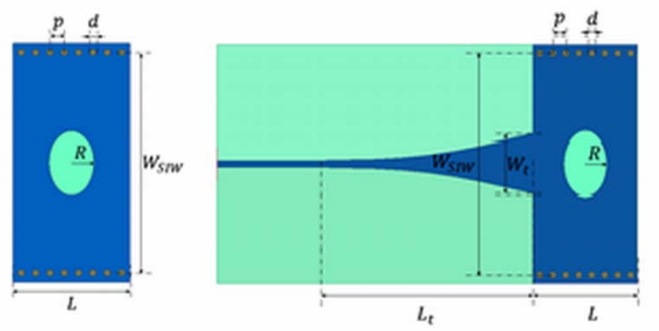

(a) (b)

Fig. 3. Two sections for the design of the Chebyshev stepped impedance band-pass SIW filter. (a) Impedance inverter with two SIW lines of length $L/2$. (b) Impedance inverter with two SIW lines of length $L/2$and an exponential microstrip-to-SIW transition.

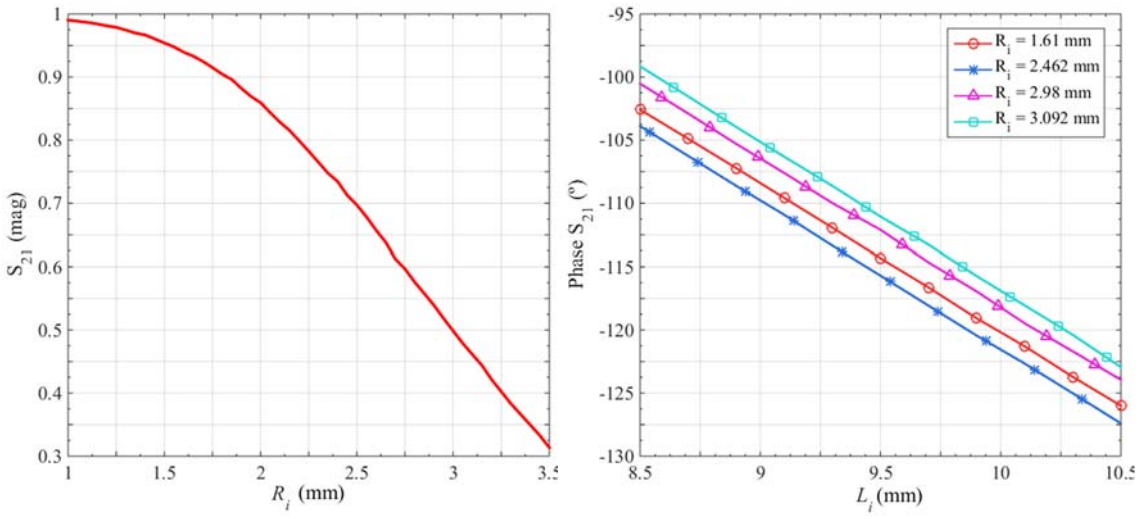

(a) (b)

Fig. 4. Parameters obtained from the design process of the section (impedance inverter without transition) shown in Fig. 3(a). (a) Magnitude of $|S_{21}|$ as a function of the parameter R_i. (b) Phase of S_{21} as a function of the section length L_i for different values of R_i.

This design process is separately applied to the different sections of the sixth-order band-pass filter (Fig. 1). Thus, the sixth-order Chebyshev stepped impedance filter synthesized by means of seven inverters (Fig. 2(b)) is divided in five internal sections as the ones shown in Fig. 3(a) and two external sections as the ones shown in Fig. 3(b), corresponding to the first/last impedance inverters. A final optimization is applied to slightly tune the response of the filter with the initial design specifications (Table 1).

3. Analysis and experiment results

Several sixth-order Chebyshev stepped impedance band-pass SIW filters were designed in this paper with the initial specifications shown in Table 1 to study the performance of circular and elliptic patterns, radiation effects and design technique described in Section 2 and [27]. The width W_{SIW} of the SIW line was optimized by means of equation (1) [4] to ensure a 20 dB lower cut-off frequency of the pass-band at $f_{c,L}$ = 3 GHz. Only two band-pass SIW filters were fabricated and measured. Both are sixth-order Chebyshev stepped impedance band-pass SIW filters with elliptic patterns etched on the top side. The first band-pass SIW filter (Fig. 5(a)) was designed using ideal waveguide ports, and then it was connected to tapered microstrip-to-SIW transitions, which were designed separately. This design is considered as the base-line filter for comparisons. The dimensions of this base-line filter (Fig. 5(a)) are included in Table

3. The second band-pass SIW filter (Fig. 5(b)) was designed by using the technique proposed in Section 2 for the first and last impedance inverters. Consequently, this design method integrates the exponential microstrip-to-SIW transitions as part of the first and last impedance inverters. The dimensions of this second band-pass SIW filters (Fig. 5(b)) are indicated in Table 4. Both band-pass SIW filters were fabricated on an Arlon AD1000 substrate by using a milling machine. The characteristics and dimensions of the used Arlon AD1000 substrate are: ε_r = 10.2, tgδ = 0.0023 at 10 GHz, substrate thickness h = 0.635 mm and copper thickness t = 0.017 mm. The measurements of the two fabricated band-pass SIW filters were carried out by means of a vector network analyzer between 0.01 GHz and 7 GHz.

(a)

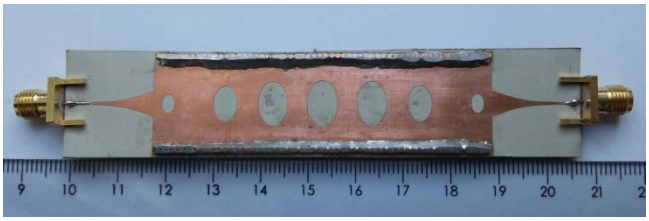

(b)

Fig. 5. Photographs of the fabricated 6-order Chebyshev stepped impedance band-pass SIW filters. (a) Initial design method with tapered microstrip-to-SIW transitions (base-line filter). (b) Alternative design approach with integrated exponential microstrip-to-SIW transitions. Dimensions are defined in Tables 3 and 4.

Table 3

Dimensions of the band-pass SIW filter shown in Fig. 5(a) (base-line filter).

Parameter	Value (mm)	Parameter	Value (mm)
R_1	1.61	L_t	24.895
R_2	2.462	L_m	5
R_3	2.98	W_{SIW}	19.4
R_4	3.092	W_m	0.612
L_1	9.219	W_t	4.866
L_2	9.439	p	1.2
L_3	9.519	d	0.6
L_4	9.843	h	0.635

Table 4

Dimensions of the band-pass SIW filter shown in Fig. 5(b).

Parameter	Value (mm)	Parameter	Value (mm)
R_1	1.3	L_t	13
R_2	2.45	L_m	5
R_3	3.05	W_{SIW}	19.4
R_4	3.158	W_m	0.612
L_1	3	W_t	5.374
L_2	11.846	p	1.2
L_3	9.946	d	0.6
L_4	10.24	h	0.635

3.1. Pattern analysis

Fig. 6 shows EM frequency responses for two sixth-order Chebyshev stepped impedance band-pass SIW filters with circular and elliptic patterns. Both band-pass SIW filters were designed with the technique described in this paper. The frequency responses of both band-pass SIW filters have cut-off frequencies in good agreement with the initial design specifications: $f_{c,L}$ = 3 GHz and $f_{c,H}$ = 3.9 GHz. As it can be seen in Fig. 6, the band-pass SIW filter with elliptic patterns has better spurious free-range performance than the band-pass SIW filter with circular patterns. In fact, the filter with elliptic patterns has the first spurious band about 0.7 GHz higher than the filter with circular patterns. In addition, it has been verified that the size of the band-pass SIW filter with elliptic patterns is smaller by 9.2 % than that with circular patterns. These two characteristics show the advantages of the first design strategy proposed in this paper, which consists of using elliptic patterns instead of circular patterns to implement the impedance inverters of the filter.

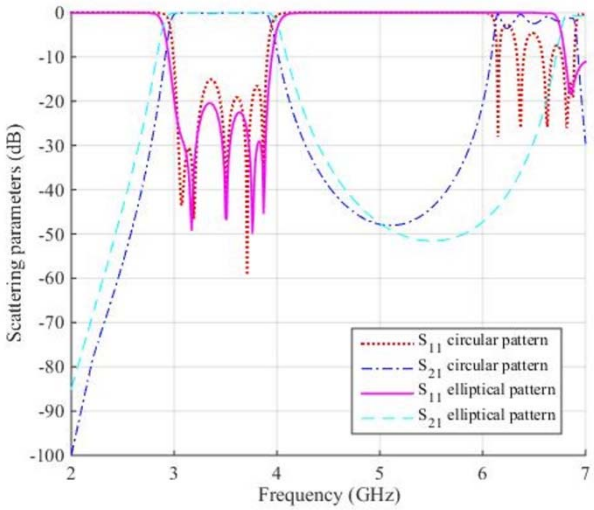

Fig. 6. EM frequency responses for sixth-order Chebyshev stepped impedance band-pass SIW filters with circular and elliptic patterns.

3.2. Measurement and design technique analysis

Figs. 7 and 8 display the EM simulation and measured frequency responses of the fabricated sixth-order Chebyshev stepped impedance band-pass SIW filters shown in Figs. 5(a) and 5(b), respectively. The band-pass filter in Fig. 5(a) was designed with ideal ports, and then it was connected to optimized tapered microstrip-to-SIW transitions (base-line filter). On the contrary, the second design strategy considered in this paper has consisted of replacing the tapered microstrip-to-SIW transitions by exponential microstrip-to-SIW transitions. These exponential microstrip-to-SIW transitions are integrated in the design technique proposed in Section 2, as part of the first and last impedance inverters of the band-pass SIW filter shown in Fig. 5(b).

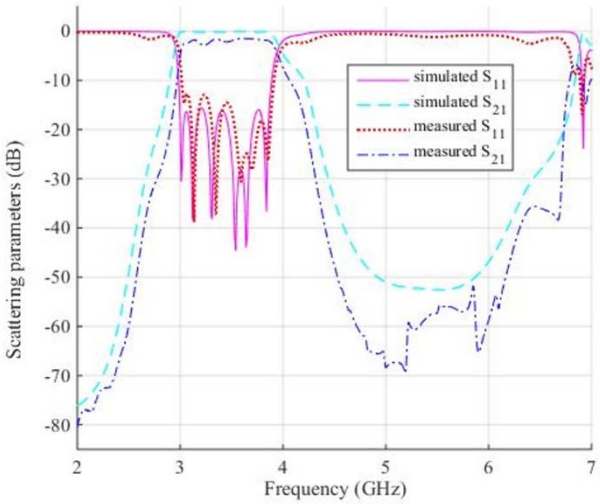

Fig. 7. EM simulation and measured frequency responses of the sixth-order Chebyshev stepped impedance band-pass SIW filter (Fig. 5(a)) with elliptic patterns and tapered microtrip-to-SIW transitions. The filter and transitions were designed separately (base-line filter).

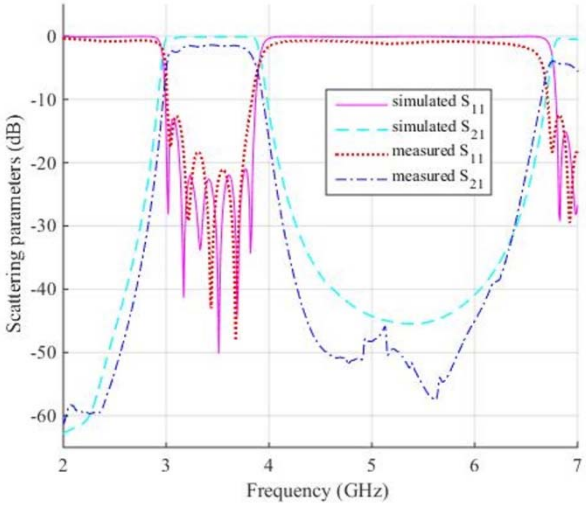

Fig. 8. EM simulation and measured frequency responses of the sixth-order Chebyshev stepped impedance band-pass SIW filter (Fig. 5(b)) with elliptic patterns and exponential microtrip-to-SIW transitions. Design obtained by integrating the exponential transitions with the first and last inverters.

As it can be seen in Figs. 7 and 8, the EM and measurement results are in good agreement with the initial design specifications (Table 1). The measured frequency responses of both band-pass SIW filters (Figs. 7 and 8) show two main characteristics. The first one is because of the SIW line, which has a high-pass frequency response. This response defines the lower cut-off frequency of the pass-band. Their value at 20 dB is $f_{c,L}$ = 3 GHz. The second behavior is due to the elliptic patterns. They implement an upper cut-off frequency in the pass-band of the filter. The value of this upper cut-off frequency at 20 dB is $f_{c,H}$ = 3.9 GHz. Insertion loss in the pass-band is 1.5 dB for both band-pass SIW filters, which includes the extra loss of the SMA connectors. In Fig. 7, we can observe that the return loss performance of the base-line filter (Fig. 5(a)) is degraded by the incorporation of the tapered microstrip-to-SIW transitions, obtaining a level better than 12 dB. Except for frequencies close to the SIW cut-off, where the waveguide exhibits high dispersion, the return loss of the second filter (Fig. 5(b)) is clearly improved, obtaining a level better than 18 dB in most of the useful bandwidth. The measured response of this second filter only shows four poles in the imaginary frequency axis. This is because two of them become complex due to probably a slight variation between the distances of the two external and five internal elliptic patterns (Fig. 5(b)), which was caused by micromachining errors. In any case, the results clearly confirm that the second band-pass filter (Fig. 8), designed with the proposed method in Section 2, has better return loss performance as compared to the base-line filter (Fig. 7). This is because in the base-line structure, the band-pass SIW filter and the tapered microstrip-to-SIW transitions were designed separately. The incorporation of the transitions at a later stage considerably degrades the performance of the initial filter. However, in the second band-pass SIW filter (Fig. 8), the effect of the exponential microtrip-to-SIW transitions was included in the design method, as part of the first and last impedance inverters of the filter (second design strategy), thus improving the return loss performance. Both band-pass SIW filters (Figs. 7 and 8) have a good behavior in

the rejection band. The rejection level is greater than 45 dB and the bandwidth at 20 dB is 2.5 GHz.

Another advantage of the second design strategy can be observed by comparing the sizes of the both band-pass SIW filters shown in Fig. 5. The size of the base-line filter (Fig. 5(a)) is 135 mm, while the size of the second filter (Fig. 5(b)) is only 105 mm. This reduction in size is mainly attributed to shorter transitions. In fact, the performance of the transitions in the second filter (Fig. 5(b)) can be poor, as the extra reflections introduced are absorbed in the first and last impedance inverters. Consequently, the transitions can be made shorter in the second filter (Fig. 5(b)) as compared to the base-line filter (Fig. 5(a)), leading to an effective reduction of the total size of the filter.

Table 5 provides a comparison between the sixth-order Chebyshev stepped impedance band-pass SIW filter with elliptic patterns and exponential microtrip-to-SIW transitions (Fig. 8) and other previously reported band-pass SIW filters implemented by means of EBGs, DGS, PSs, resonators and CSRRs [11-26]. The band-pass response of the EBG structures [11-14] is obtained from the high-pass characteristic of the SIW line together with the wide stop-band behavior of the periodic patterns. Some resonator-based structures [17,20-25] use a similar design method, which combines high-pass and stop-band characteristics. This design method allows to carry out band-pass SIW filters with different bandwidths (small or large). However, it is not computationally efficient, since in order to obtain the pass-band according to the initial design specifications, the filter structures, usually 3D, has to be optimized by using a 3D EM simulator needing a lot of computational time. The other design methods can implement band-pass SIW filters with small (FBW < 10 %) [15,16] and large (FBW < 21 %) [18,19] bandwidths. The small bandwidths are obtained by means of design methods using lumped-element equivalent circuits with *LC* resonators only valid in a narrow band, while the large bandwidths are defined from more rigorous design methods using impedance inverters and

$\lambda_g/2$ distributed resonators. These methods become very sensitive when the order of the band-pass filter to be designed increases. The proposed technique for the *n*-order Chebyshev stepped impedance band-pass SIW filter design is simpler than these previous design methods. Based on a rigorous synthesis, using transmission lines and impedance inverters, it is less sensitive and allows a better control of the bandwidth and return loss than the design methods using *LC* [15,16] and $\lambda_g/2$ [18,19] resonators. In addition, the proposed technique has the ability to design wide band-pass SIW filters as compared to the design procedures based on lumped-element resonators [15,16]. As it can be seen in Table 5, the fractional bandwidth (FBW) is 29% for the proposed design, while it varies between 18.9% and 61.2% for the band-pass SIW filters designed with EBGs, 6.5% and 61.7% for stop-band resonators and 5.1% and 20.9% for band-pass resonators. The return loss (*RL*) and size also depend of the structure type and design technique used, and the number of cells in cascade. Except for the band-pass SIW filters loaded with compact microstrip resonant cells (CMRC) [20] and based on perforated sections (PSs) [18], the proposed design presents better return loss (*RL*) than the others. In addition, it does not have the largest size, considering some designs with a smaller number of cascaded cells [15,16,19,21,23,24].

Table 5

Comparison between the designed band-pass SIW filters and other band-pass SIW filters implemented by means of EBGs, DGSs, resonators and CSRRs.

Reference	Type–No of cells	Design method	f_0 (GHz)	FBW (%)	*IL* (dB)	*RL* (dB)	2-D size ($\lambda_0 \times \lambda_0$)
[11] Fig. 22	EBG–11	Periodic structure	12.2	61.2	1.3	10	0.52×1.24
[12] Fig. 16	EBG–9	Periodic structure	2.7	74	0.5	9	0.29×0.75
[13] Fig. 10	EBG–13	Periodic structure	6.6	30.3	1.25	5.8	0.23×1.38
[14] Fig. 3(a)	EBG–9	Periodic structure	3.4	18.9	1.4	12.3	0.24×0.75
[15] Fig. 12	DGS–4	Band-pass resonators	5.88	5.1	1.38	15	0.42×2.05
[16] Fig. 7	DGS–2	Band-pass resonators	4.9	9.2	1.1	18	0.39×0.39
[17] Fig. 5	DGS-3	Stop-band resonators	10	23	1.2	20	0.22×0.45
[18] Fig. 6	PS-5	Band-pass resonators	3.65	17.7	1.31	18	0.21×0.98
[19] Fig. 7	PS-6	Band-pass resonators	4.5	20.9	1.5	14.5	0.25×1.15
[26] Fig. 15	OCSRR-2	Band-pass resonators	5.47	6.9	2	10	0.13×0.33
[20] Fig. 12	CMRC–3	Stop-band resonators	4.54	30.6	1.2	22	0.14×0.73
[21] Fig. 18	SHR–2	Stop-band resonators	12.5	47	1.1	10	1.12×1.96
[22] Fig. 15(b)	CSRR–6	Stop-band resonators	5.05	6.5	2	17	0.2×0.43
[23] Fig. 3	CSRR–6	Stop-band resonators	9.46	29.7	1	16	0.63×0.75
[24] Fig. 4	DESRR–3	Stop-band resonators	9.4	61.7	1.5	9	0.37×1.0
[25] Fig. 19(c)	SIR–4	Stop-band resonators	1.7	9.4	1.8	13	0.09×0.17
This work Fig. 8	Ellipse-7	Stepped impedance	3.45	29	1.5	18	0.22×1.2

where f_0 is the central frequency; FBW is the fractional bandwidth; *IL* and *RL* are, respectively, insertion and return losses at f_0; and λ_0 is free-space wavelength.

3.3. Radiation analysis

The designed sixth-order Chebyshev stepped impedance band-pass SIW filter can cause radiation loss due to the elliptic patterns etched on the top SIW surface. To study the radiation loss, we have determined the forward loss factor F_{LF} from EM simulations as a function of frequency for the two manufactured filters (Fig. 5).

$$F_{LF} = 1 - |S_{11}|^2 - |S_{21}|^2 \quad (6)$$

The conductors and substrate were respectively considered perfect and lossless in the EM simulations to find out only the radiation losses. As it can be seen in Fig. 9, radiation losses were obtained for the two manufactured filters with tapered and exponential microstrip-to-SIW transitions as comparative study. Three different frequency regions can be identified in Fig. 9. The first one includes two frequency ranges: 2 GHz – 3 GHz and 3.9 GHz – 6.75 GHz. The second one is between 3 GHz and 3.9 GHz. Finally, the last region appears at frequencies above 6.75 GHz. The radiation losses are small for the first two regions. In the first region, the radiation losses vary between 0 and 5 %. This does not occur in the second region (3 GHz – 3.9 GHz), which corresponds to the pass-band of both filters. The radiation losses are quasi-constant and are below 3 %. In the last region, radiation losses increase, due to the appearance of the first spurious band. It can be observed that radiation losses are similar in both filters for the first two regions. However, in the third region (corresponding to the spurious band) the base-line filter (with tapered microstrip-to-SIW transitions) exhibits higher radiation losses.

This is probably because the microstrip-to-SIW transitions are longer in the base-line filter (Fig. 5(a)) as compared to the second filter (Fig. 5(b)).

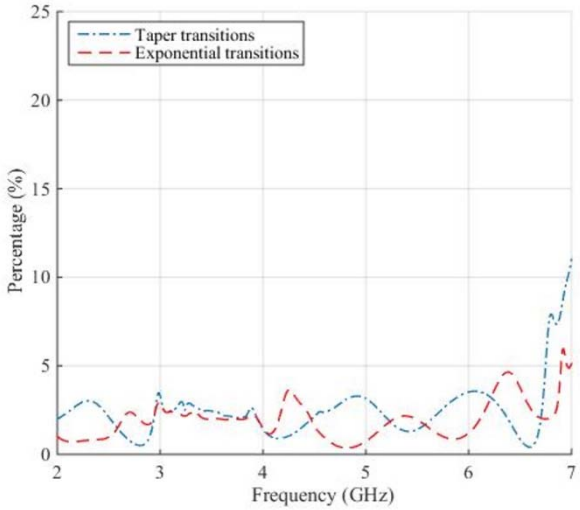

Fig. 9. Forward loss factor (%) for the two manufactured sixth-order Chebyshev stepped impedance band-pass SIW filters as a function of the frequency.

4. Conclusion

A high-performance sixth-order Chebyshev stepped impedance band-pass substrate integrated waveguide (SIW) filter using elliptic patterns and exponential microstrip-to-SIW transitions has been designed and measured for the first time in this paper. First, it has been shown that elliptic patterns in comparison with circular patterns exhibit larger spurious free ranges and lower sizes. Second, the paper has demonstrated that the filter performance can be considerably improved if the microstrip-to-SIW transitions are integrated as part of the design process. As added benefit, the transitions can be made shorter, as the extra reflections introduced by them are absorbed in the input/output impedance inverters. Consequently, size can be further reduced. Measured results have shown the effectiveness of the proposed design technique in

improving the performance of the sixth-order Chebyshev band-pass SIW filter, as compared to a base-line filter which performs the design of the main structure and transitions separately.

5. Acknowledgment

The authors gratefully acknowledge financial support from Ministerio de Economía y Competitividad of Spain, Fundación Séneca of Región de Murcia and the European Regional Development Funds for the financial support (grant no.: TEC2016-75934-C04-4-R and PRX18/00092).

References

[1] Boria VE, Gimeno B. Waveguide filters for satellites. IEEE Microwave Mag 2007; 8: 60-70.

[2] Uchimura H, Takenoshita T, Fujii M. Development of a laminated waveguide. IEEE Trans Microw Theory Tech 1998; 46: 2438-2443.

[3] Deslandes D, Wu K. Integrated microstrip and rectangular waveguide in planar form. IEEE Microw Wirel Compon Lett 2001; 11: 68-70.

[4] Cassivi Y, Perregrini L, Arcioni P, Bressan B, Wu K, Gonciauro G. Dispersion characteristics of substrate integrated rectangular waveguide. IEEE Microw Wirel Compon Lett 2002; 12: 333-335.

[5] Deslandes D, Wu K. Single-substrate integration technique of planar circuits and waveguide filters. IEEE Trans Microw Theory Tech 2003; 51: 593-596.

[6] Wu K, Deslandes D, Cassivi Y. The substrate integrated circuits – A new concept for high-frequency electronics and optoelectronics. In: International Conference on Telecommunications in Modern Satellite, Cable and Broadcasting Service (TELSIKS), 1-3 Oct 2003, 2-9.

[7] Xu F, Wu K. Guided-wave and leakage characteristics of substrate integrated waveguide. IEEE Trans Microw Theory Tech 2005; 53: 66-73.

[8] Deslandes D, Wu K. Accurate modeling, wave mechanism, and design considerations of a substrate integrated waveguide. IEEE Trans Microw Theory Tech 2006; 54: 2516-2526.

[9] Lai Q, Fumeaux C, Hong W, Vahldieck R. Characterization of the propagation properties of the half-mode substrate integrated waveguide. IEEE Trans Microw Theory Tech 2009; 57: 1996-2004.

[10] Bozzi M, Georgiadis A, Wu K. Review of substrate-integrated waveguide circuits and antennas. IET Microw Antennas Propag 2010; 5: 909-920.

[11] Hao ZC, Chen JX, Chen XP, Wu K. Compact super-wide bandpass substrate integrated waveguide (SIW) filters. IEEE Trans Microw Theory Tech 2005; 53: 2968-2977.

[12] Wu LS, Zhou XL, Yin WY, Liu CT, Zhou L, Mao JF, Peng HL. A new type of periodically loaded half-mode substrate integrated waveguide and its applications. IEEE Trans Microw Theory Tech 2010; 58: 882-893.

[13] Moitra S, Bhowmik PS. Modelling and analysis of substrate integrated waveguide (SIW) and half-mode SIW (HMSIW) band-pass filter using reactive longitudinal periodic structures. AEU-Int J Electron Commun 2016; 70, 1593-1600.

[14] Ruiz JD, Martínez-Viviente FL, Alvarez-Melcon A, Hinojosa J. Substrate integrated waveguide (SIW) with Koch fractal electromagnetic bandgap structures (KFEBG) for bandpass filter design. IEEE Microw Wirel Compon Lett 2015; 25: 160-162.

[15] Zhang YL, Hong W, Chen JX, Tang HJ. Novel substrate integrated waveguide cavity filter with defected ground structure. IEEE Trans Microw Theory Tech 2005; 53: 1280-1287.

[16] Shen W, Yin WY, Sun XW. Compact substrate integrated waveguide (SIW) filter with defected ground structure. IEEE Microw Wirel Compon Lett 2011; 21: 83-85.

[17] Wang C, Wang Z, Huang Y M. Size-miniaturized half-mode substrate integrated waveguide bandpass filter incorporating E-shaped defected ground structure for wideband communication and radar applications. 20th International Conference on Advanced Communication Technology (ICACT), 2018. IEEE; 2018. p. 12-16.

[18] Silvestri L, Massoni E, Tomassoni C, Coves A, Bozzi M, Perregrini L. Substrate integrated waveguide filters based on a dielectric layer with periodic perforations. IEEE Trans Microw Theory Tech 2017; 65: 2687–2697.

[19] Coves A, Torregrosa G, Vicent G, Bronchalo E, San Blas AA, Bozzi M. Analysis of a perforated SIW structure with a rectangular air box and its application to the design of a step-impedance microwave filte. 32nd General Assembly and Scientific Symposium of the International Union of Radio Science (GASS), 2017. URSI; 2017. p. 1-4.

[20] Huang L, Wu W, Zhang X, Lu H, Zhou Y, Yuan N. A novel compact and high performance bandpass filter based on SIW and CMRC technique. AEU-Int J Electron Commun 2017; 82, 420-425.

[21] Khorand T, Bayati MS. Novel half-mode substrate integrated waveguide bandpass filters using semi-hexagonal resonators. AEU-Int J Electron Commun 2018; 95, 52-58.

[22] Dong YD, Yang T, Itoh T. Substrate Integrated waveguide loaded by complementary split-ring resonators and its applications to miniaturized waveguide filters. IEEE Trans Microw Theory Tech 2009; 57: 2211-2222.

[23] Deng K, Guo Z, Li C, Che W. A compact planar bandpass filter with wide out-of-band rejection implemented by substrate integrated waveguide and complementary split-ring resonator. Microw Opt Techno Lett 2011; 53: 1483-1487.

[24] Norooziarab M, Atlasbaf Z, Farzami F. Substrate integrated waveguide loaded by 3-dimensional embedded split ring resonator. AEU-Int J Electron Commun 2014; 68, 658-660.

[25] Danaeian M, Afrooz K, Hakimi A. Miniaturization of substrate integrated waveguide filters using novel compact metamaterial unit-cells based on SIR technique. AEU-Int J Electron Commun 2018; 84, 62-73.

[26] Danaeian M, Afrooz K, Hakimi A, Moznebi AR. Compact bandpass filter based on SIW loaded by open complementary split-ring resonators. Int. J. RF Microw. Comput.-Aided Eng. 2016; 26: 674-682.

[27] Cameron RJ, Kudsia CM, Mansour R. Microwave filters for communication systems: Fundamentals, design, and applications. Hoboken: Wiley; 2007.

[28] Deslandes D. Design equations for tapered microstrip-to-substrate integrated waveguide transitions. In: IEEE MTT-S International Microwave Symposium, 23-28 May 2010, 704-707.